AIAA JOURNAL
Vol. 39, No. 7, July 2001

Rotordynamic Effects of Compressor Rotor-Tip Clearance Asymmetry

Seung Jin Song*
Seoul National University, Seoul 151-742, Republic of Korea
and
Kil Yong Park†
Inha University, Inchon 402-751, Republic of Korea

Rotordynamic effects caused by nonaxisymmetric rotor-tip clearance in an axial compressor stage have been analyzed. Two coupled actuator disc analyses are carried out at blade (meridional plane) and radius (radial plane) scales. Continuity, axial, and tangential momentum equations are used to connect upstream and downstream flows across the compressor stage, and a small perturbation analysis is used to obtain flowfield nonuniformities. Predictions indicate the following. Relative to the passage flow, the flow associated with the rotor-tip clearance is axially retarded and tangentially underturned. Furthermore, the compressor blades near the smaller tip gap are more highly loaded. Thus, the tangential force asymmetry promotes a backward whirl. However, the pressure asymmetry caused by azimuthal flow redistribution induces a forward whirl. The net result is a backward-whirling force whose magnitude is much smaller than that of the forward-whirling force found in turbines.

Nomenclature

B = Bernoulli constant
C = absolute flow velocity
c = axial blade chord
c_l = lift coefficient
e = magnitude of rotor offset
F_x = lateral force in the direction of the offset
F_y = lateral force perpendicular to the direction of the offset
f_y = tangential force per azimuthal length
H = annulus height
H_b = rotor blade span
h = enthalpy
L = rotor thickness
$\dot{m}$ = mass flux
P = pressure
Q = strength of the shear layer
q = nondimensional vorticity strength; local mass flux
R = mean compressor radius; turbine reaction
s = blade pitch
t = radial tip clearance
U = turbine rotational speed at the mean radius, ωR
W = relative velocity
X = direction along the rotor offset
x = axial direction
Y = direction perpendicular to rotor offset
y = tangential direction
z = radial direction
α = absolute flow angle, eigenvalue
α_x = direct excitation force coefficient
α_y = cross excitation force coefficient
β = relative flow angle; angle between tip jet flow and passage flow
Δ = thickness of underturned layer downstream of actuator disc
Φ = turbine flow coefficient, C_x/U
θ = azimuthal angle measured in the direction of rotation from the minimum gap location; angle between the underturned stream and the bladed stream
λ = nondimensional mass fraction of underturned flow
ρ = density
Ψ = meridional stream function; work coefficient
ω = angular velocity of rotor shaft rotation; vorticity

Subscripts

D = design value
m = mean
t = stagnation condition
0 = far upstream of actuator disc in the blade scale analysis
$0-$ = near upstream of the actuator disc in the radius scale analysis
$0+$ = near downstream of the actuator disc in the radius scale analysis
1 = rotor inlet in the blade scale analysis
2 = stator inlet in the blade scale analysis
3 = stator outlet in the blade scale analysis
4 = far downstream of stator in the blade scale analysis
$\perp$ = meridional component

Superscripts

$-$ = the part of flow downstream that has crossed the bladed part of turbine flow
$+$ = the part of flow downstream that was underturned due to the rotor tip gap
$'$ = nonaxisymmetric perturbation
$\bar{}$ = azimuthal mean, or axisymmetric value
$\hat{}$ = complex amplitude

I. Introduction

THE effects of nonaxisymmetric tip clearance on the performance and rotordynamics of axial turbomachinery have been investigated by various authors. In turbines the rotordynamic forces were first suggested independently by Thomas[1] and Alford.[2] They both assumed that the blades in the smaller gap region are more

Received 4 June 1999; revision received 1 July 2000; accepted for publication 29 November 2000.

*Assistant Professor, School of Mechanical and Aerospace Engineering.
†Research Assistant, Department of Aerospace Engineering.

highly loaded. The net effect is a cross-coupled force acting perpendicularly to the rotor offset in the direction of rotation, causing a forward whirl. Experimentally, Ulrichs[3] and Martinez-Sanchez et al.[4] obtained rotordynamic force and aerodynamic data for unshrouded turbines. Analytically, Qiu[5] formulated an actuator disk turbine model based largely on the compressor model of Horlock and Greitzer.[6] However, the assumption of perfect flow guidance in the tip clearance region led to poor predictions. Song and Martinez-Sanchez[7,8] presented an actuator disk analysis capable of accurately predicting forces measured in turbines.

On the other hand, research on the effects of nonaxisymmetric rotor-tip clearance in axial compressors has been relatively scarce. Experimentally, Vance and Laudadio[9] measured forces in an axial fan. Analytically, Alford[2] assumed that, in compressors, blades near the smaller gap are more lightly loaded, and, thus, predicted a backward whirl inducing force. Horlock and Greitzer[6] examined the effect of clearance asymmetry on the velocity field. Colding-Jorgensen[10] adapted Qiu's analysis[5] for a compressor and predicted forward whirling forces in the "normal operating range." Ehrich[11] used the parallel compressor model and data from the General Electric Low Speed Research Compressor to predict mostly backward whirling forces. Recently, Graf et al.[12] developed a model to predict the effects of clearance asymmetry on compressor stability.

Despite such efforts, flowfields and rotordynamic forces induced by rotor-tip clearance asymmetry in an axial compressor are not well understood. If one assumes, as Alford did, that the blades near the smaller tip gap are more lightly loaded, a forward-whirl-inducing force results. However, if one assumes, as Ehrich did, that the blades near the smaller tip gap are more highly loaded, a backward-whirl-inducing force results. Furthermore, the effects of nonaxisymmetric flow redistribution have not yet been addressed by anyone. Thus, neither direction nor magnitude of such forces can be predicted with confidence (Fig. 1).

Therefore, the objective of this investigation is to gain physical understanding of flowfields and rotordynamic effects induced by static, nonaxisymmetric rotor-tip clearance in a single-stage axial compressor. An analytical compressor model based on actuator disk theory has been newly formulated. From the model's flowfield predictions the rotordynamic forces can be inferred.

II. Analytical Model

The approach taken in this investigation is conceptually similar to that adopted in Song and Martinez-Sanchez.[7,8] The blade scale analysis solves for the radial flow redistribution caused by axisymmetric rotor-tip clearance. The radius scale analysis examines the azimuthal flow redistribution induced by nonaxisymmetric rotor-tip clearance.

The actuator disk consists of a compressor stage with a full-span inlet guide vane (IGV) row, a partial-span rotor row, and a full-span stator row, collapsed into a single plane at $x = 0$. The various axial locations at the blade scale are as follows. Upstream of the IGV is referred to as station 0. Inlet to the rotor is referred to as station 1, and the rotor exit is called station 2. Downstream of the stator row is called station 3. Far downstream is referred to as station 4. On the radius scale $x = 0-$ is equivalent to the blade scale station 0, and $x = 0+$ is equivalent to the blade scale station 4. Figure 2 shows the blade scale and the radius scale views of the actuator disk. Figure 3 shows compressor blade geometry with the velocity triangles from Cohen et al.[13]

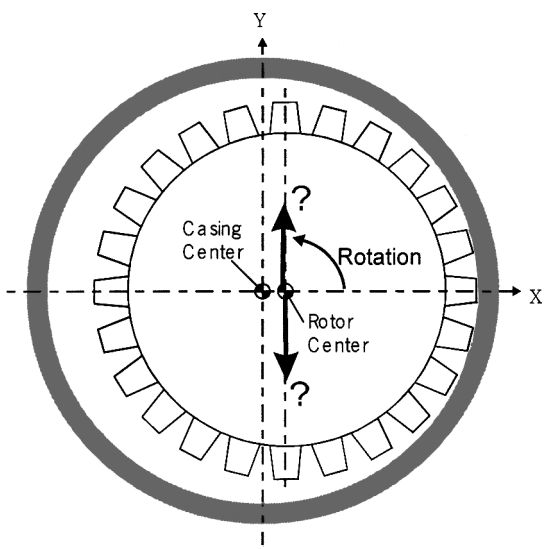

Fig. 1 Lateral force on an offset compressor rotor.

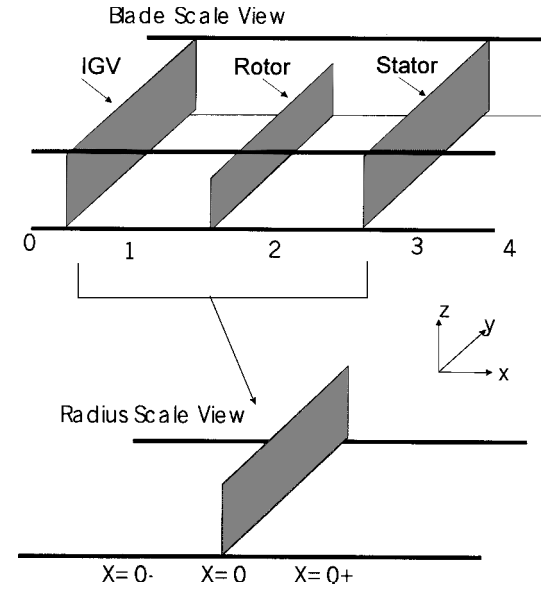

Fig. 2 Blade and radius scale views of a compressor stage.

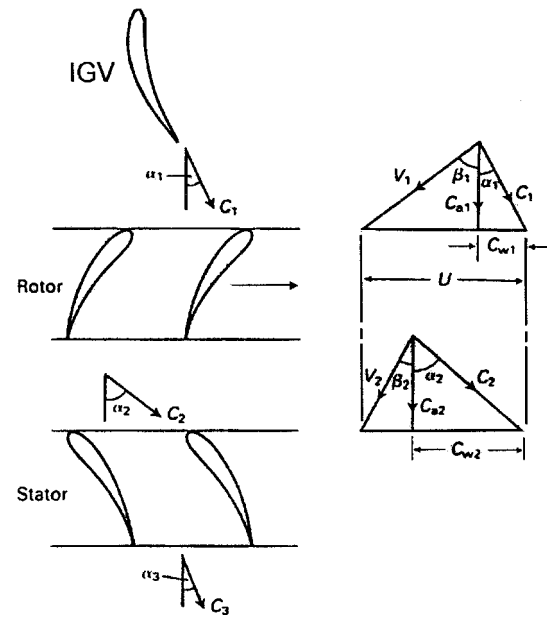

Fig. 3 Compressor velocity triangles.[13]

The assumptions used in the analysis are listed here: 1) incompressible, inviscid flow; 2) compressor stage collapsed in the axial direction to $x = 0$; 3) the blade geometry is radially uniform, except for the rotor-tip clearance; and 4) in the bladed region away from tip clearance, the blades guide the flow perfectly, or the relative flow angles are same as the blade angles. Because of assumptions 1 and 4, the effects such as deviation and blockage are not accounted for in this model.

The current approach is different from the preceding nonaxisymmetric compressor models in the following ways. First, empirical inputs are not needed. Approaches of Horlock and Greitzer[6] and Colding-Jorgensen[10] both require empirical performance (e.g.,

pressure rise coefficient, efficiency) variation with clearance. Ehrich's[11] method requires detailed aerodynamic data, and Graf's[12] approach requires compressor characteristics. However, the models of Horlock and Greitzer[6] and Graf[12] consider more complex physics such as deviation in the passage and compressor stability, which are not modeled in the current model. Second, the current model explicitly accentuates the effects of rotor-tip clearance by transforming to a streamline coordinate from the radial z coordinate. Song and Martinez-Sanchez[8] showed that it was important to explicitly model the flow associated with the tip region. Qiu[5] uses experimentally determined dependence of global parameters (e.g., pressure rise coefficient or efficiency) on tip clearance as inputs in his model. Such smearing of the tip clearance leads to poor predictions. Colding-Jorgensen's[10] is similar to that of Qiu.[5]

A. Blade Scale Analysis

The compressor blade scale analysis presented here is based on the work of Roh.[14] The additional assumptions for the blade scale analysis are as follows:

1) The flow is axisymmetric $\partial/\partial y = 0$.

2) Flow conditions are radially uniform at the rotor inlet (station 1).

Because there are no variations with y, the azimuthal momentum equation for the flow is

$$\boldsymbol{C}_\perp \cdot \nabla C_y = 0 \tag{1}$$

where $\boldsymbol{C}_\perp$ is the meridional velocity defined as

$$\boldsymbol{C}_\perp = \boldsymbol{i}C_x + \boldsymbol{k}C_z$$

In this case the vorticity equation can be written as

$$\boldsymbol{C}_\perp \cdot \nabla \omega_y = 0, \qquad \left(\omega_y = \frac{\partial C_x}{\partial z} - \frac{\partial C_z}{\partial x}\right) \tag{2}$$

and the Bernoulli equation becomes

$$\boldsymbol{C}_\perp \cdot \nabla B_\perp = 0, \qquad \left(B_\perp = P/\rho + \tfrac{1}{2}C_\perp^2\right) \tag{3}$$

The stream function Ψ can be introduced for the meridional flow to obtain

$$\omega_y(\Psi) = \nabla_\perp^2 \Psi \left(\nabla_\perp^2 = \frac{\partial^2}{\partial x^2} + \frac{\partial^2}{\partial z^2}\right) \tag{4}$$

Upstream of the stage ($x < 0$) the flow is assumed to be irrotational ($\omega_y = 0$). Therefore, Ψ obeys Laplace's equation. Downstream ($x > 0$), according to Gauthier,[15] the axial velocity at the rotor exit can be assumed to piecewise constant, with a discontinuity at the blade tip. Therefore, the ω_y vorticity is concentrated at their interface. Quantities in the underturned layer are denoted with a $()^+$ superscript, and those in the rotor blade region by a $()^-$ superscript.

Because

$$\omega_y = \frac{\mathrm{d}B_\perp}{\mathrm{d}\Psi} \tag{5}$$

vorticity ω_y is created and then convected along each streamline. From the definition of $B_\perp$ with the continuity constraint and the assumption of spanwise uniform blading,

$$B_{\perp 3} - B_{\perp 1} = (P_3 - P_1)/\rho \tag{6}$$

Upstream of the stage, the irrotationality means $\mathrm{d}B_{\perp 1}/\mathrm{d}\Psi = 0$. Therefore, Eq. (5) can be rewritten as

$$\omega_{y3} = \frac{\mathrm{d}B_{\perp 3}}{\mathrm{d}\Psi} = \frac{\mathrm{d}(B_{\perp 3} - B_{\perp 1})}{\mathrm{d}\Psi} = \frac{\mathrm{d}}{\mathrm{d}\Psi}\left(\frac{P_3 - P_1}{\rho}\right) \tag{7}$$

Thus, ω_y can be determined from the static enthalpy $(P_3 - P_1)/\rho$ addition by the compressor.

The static pressure rise is equivalent to the stagnation enthalpy increase, given by Euler's equation, minus the kinetic energy gain.

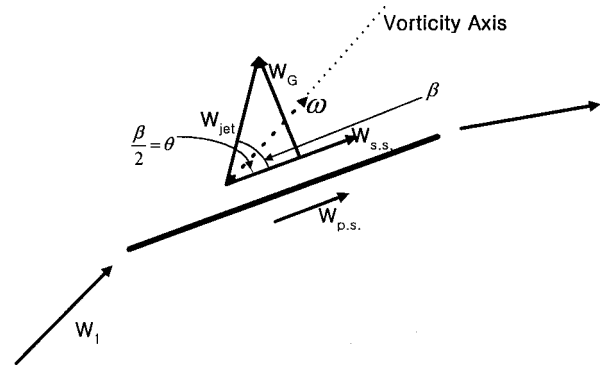

Fig. 4 Schematic of the compressor tip clearance model.[14]

The static pressure rise for any streamline, which crosses the disk, can be obtained as

$$(\Delta P_{13}/\rho) = \Delta h_t - \Delta K.E. \tag{8}$$

where $\Delta P_{13} = P_3 - P_1$, $\Delta h_t = U(C_{y2} - C_{y1})$ and $\Delta K.E. = \frac{1}{2}(C_3^2 - C_1^2)$. The assumptions of perfect guidance by the blades and radial uniformity lead to

$$C_{y1} = C_{x1}\tan(\alpha_1) \tag{9}$$

At the rotor exit (station 2) the flow has split into two streams. For the bladed stream

$$C_{y2}^- = U - C_{x2}^- \tan(\beta_2) \tag{10}$$

Therefore,

$$[(P_3 - P_1)/\rho]^- = U\left(C_{y2}^- - C_{y1}\right) - \tfrac{1}{2}\left[C_{x3}^{-2} + C_{y3}^{-2} - \left(C_{x1}^2 + C_{y1}^2\right)\right] \tag{11}$$

The tip clearance flow model (Fig. 4) used in this analysis is described in detail in Roh.[14] Basically, the tip leakage flow and an equal amount of passage flow form a tip vortex. Trajectory, strength, and mass fraction of the vortex can be determined as a function of the compressor blade geometry and tip clearance. Thus, for the underturned stream the azimuthal velocity is given as

$$C_{y2}^+ = U - C_{x2}^+ \frac{\cos(\theta)\sin(\beta_m + \theta)}{\cos(\beta_m)} \tag{12}$$

where β_m is the mean flow angle through the rotor and θ is the angle relative to β_m at which the underturned stream is assumed to roll up into vortices (Fig. 4). β_m is given by

$$\tan(\beta_m) = \tfrac{1}{2}[\tan(\beta_1) + \tan(\beta_2)] \tag{13}$$

and θ is a function of the lift coefficient per unit blade span c_l, which can determined as follows:

$$c_l = 2.0(s/c)\cos(\beta_m)[\tan(\beta_1) - \tan(\beta_2)] \tag{14}$$

where s/c is the reciprocal of solidity. Thus,

$$[(P_3 - P_1)/\rho]^+ = U\left(C_{y2}^+ - C_{y1}\right) - \tfrac{1}{2}\left(C_{x3}^{+2} + C_{y3}^{+2}\right) - \left[C_{x3}^+ \frac{\sin(\theta)}{\cos(\beta_m)}\right]^2 + \left(C_{x1}^2 + C_{y1}^2\right) \tag{15}$$

In Eqs. (14) and (15) the axial velocity C_x at the disk is a function of z. Thus, $\mathrm{d}/\mathrm{d}\Psi$ in Eq. (7) can be expressed as

$$\frac{\mathrm{d}}{\mathrm{d}\Psi} = \frac{\partial}{\partial C_x}\left(\frac{\partial C_x}{\partial z}\frac{\partial z}{\partial \Psi}\right)_{x=0} = \left(\frac{1}{C_x}\frac{\partial C_x}{\partial z}\right)_{x=0}\frac{\partial}{\partial C_x} \tag{16}$$

Then, from Eqs. (7), (11), (14), and (15), the equation for Ψ becomes the following.

Upstream ($x < 0$):

$$\nabla_{\perp}^2 \Psi = 0 \tag{17}$$

Downstream ($x > 0$):

$$\nabla_{\perp}^2 \Psi = Q\delta(\Psi - \Psi_{\text{tip}}) \tag{18}$$

where

$$Q = \int_{-}^{+} \omega_y \, \mathrm{d}\Psi = B_{\perp 3}^{+} - B_{\perp 3}^{-}$$

δ is Dirac's delta function, and Q is the strength of the y component of the vorticity between the underturned and bladed streams. From Eqs. (6), (11), and (14)

$$Q = U\left(C_{y2}^{+} - C_{y1}\right) - U\left(C_{y2}^{-} - C_{y1}\right) - \frac{1}{2}\left\{C_{y3}^{+2} + \left[C_{x3}^{+}\frac{\sin(\theta)}{\cos(\beta_m)}\right]^2 - C_{y3}^{-2}\right\} \tag{19}$$

The boundary conditions are

$$\Psi(x, 0) = 0, \qquad \Psi(x, H) = C_{x0}H$$

$$\Psi(x = 0-, z) = C_{x0}z, \qquad \frac{\partial \Psi}{\partial x}(x = 0+, z) = 0$$

$$\Psi_1(z) = \Psi_3(z), \qquad \frac{\partial \Psi_1(z)}{\partial z} = \frac{\partial \Psi_3(z)}{\partial z} \tag{20}$$

The axial velocities for each stream can be expressed as

$$C_{x2}^{+} = C_{x1}[1 + (q/2)(1 - \lambda)] = C_{x3}^{+} \tag{21}$$

$$C_{x2}^{-} = C_{x1}[1 - \lambda(q/2)] = C_{x3}^{-} \tag{22}$$

where $q = Q/C_{x1}^2$.

Substituting Eqs. (21) and (22) into the definition of Q yields a quadratic equation for Q as a function of λ:

$$\left\{G(1 - 2\lambda) - \left[\lambda\frac{\sin(\theta)}{\cos(\beta_m)}\right]^2\right\}\left(\frac{q}{2}\right)^2 + 2\left\{2 + \frac{1}{\Phi}(1 - \lambda)T + \frac{\lambda}{\Phi}\tan(\beta_2) + G - \lambda\left[\frac{\sin(\theta)}{\cos(\beta_m)2}\right]^2\right\} \times \left(\frac{q}{2}\right) + \left\{\frac{2}{\Phi}T - \frac{2}{\Phi}\tan(\beta_2) + \left[\frac{\sin(\theta)}{\cos(\beta_m)}\right]^2\right\} = 0 \tag{23}$$

where $G = \tan^2(\alpha_3) + [\sin(\theta)/\cos(\beta_m)]^2$, $T = \cos(\theta)\sin(\beta_m + \theta)/\cos(\beta_m)$. The amount of flow leaked through the tip gap is $\lambda/2$, and λ is a function of t/H and q:

$$t/H = (\lambda/2)[1 - (1 - \lambda/2)q/2] \tag{24}$$

Thus, once the values of λ and q that satisfy the system of Eqs. (23) and (24) have been found for a given t/H, the velocities can be evaluated.

B. Radius Scale Analysis

To model a compressor offset at some amplitude $\hat{e}$ much smaller than the rotor blade span H_b, a linear perturbation approximation is used. For small tip gaps ($t/R \ll 1$) with an offset rotor, the azimuthal distribution of the rotor-tip gap is given as

$$t = \bar{t} + \mathrm{Re}\left[\bar{e}\, e^{i(y/R)}\right] \tag{25}$$

where $\bar{t}$ is the mean rotor tip gap and y is the distance from maximum tip gap in the azimuthal direction (Fig. 5). This analysis is similar to the turbine radius model described in Song and Martinez-Sanchez.[8] Basically, continuity, axial, and tangential momentum equations are used to connect upstream and downstream flowfields on the radius scale. For a prescribed eccentricity perturbations in velocity and pressure are obtained via a small perturbation about the mean solution provided by the blade scale analysis. Further details of the compressor radius scale analysis can be found in Park.[16]

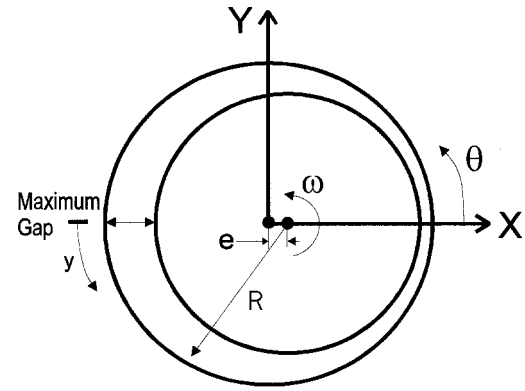

Fig. 5 Coordinate system for radius scale analysis.

C. Calculation of Rotordynamic Coefficients

The rotordynamic excitation force can be obtained from the perturbation quantities. The tangential force exerted on the compressor per azimuthal length by the fluid can be defined as

$$f_y = \lambda q\left(C_{y1} - C_{y2}^{+}\right) + (1 - \lambda)q\left(C_{y1} - C_{y2}^{-}\right) \tag{26}$$

The mean and the perturbation of f_y are, respectively,

$$\bar{f}_y = \bar{\lambda}\bar{q}\left(\bar{C}_{y1} - \bar{C}_{y2}^{+}\right) + (1 - \bar{\lambda})\bar{q}\left(\bar{C}_{y1} - \bar{C}_{y2}^{-}\right) \tag{27}$$

$$f_y' = \bar{\lambda}\bar{q}\left(\bar{C}_{y1} - \bar{C}_{y2}^{+}\right)\left[\frac{\lambda'}{\bar{\lambda}} + \frac{q'}{\bar{q}} + \frac{C_{y1}' - C_{y2}'^{+}}{\bar{C}_{y1} - \bar{C}_{y2}^{+}}\right] + (1 - \bar{\lambda}) \times \bar{q}\left(\bar{C}_{y1} - \bar{C}_{y2}^{-}\right)\left[\frac{-\lambda'}{1 - \bar{\lambda}} + \frac{q'}{\bar{q}} + \frac{C_{y1}' - C_{y2}'^{-}}{\bar{C}_{y1} - \bar{C}_{y2}^{-}}\right] \tag{28}$$

The perturbation in f_y contains the effects of nonaxisymmetry in tip leakage mass flow rate, through flow, and flow turning induced by the rotor-tip clearance asymmetry.

Another source of excitation forces is the nonaxisymmetric pressure pattern, which acts radially on the hub. Here, the pressure acting on the rotor hub is approximated as the average of pressures at stations 1 and 2 on the blade scale (inlet and exit of the rotor) $\langle P \rangle$:

$$\langle P \rangle = (P_1 + P_2)/2 = P_1 - [(P_1 - P_2)/2] \tag{29}$$

$$\langle P \rangle' = P_1' - \rho/2\left[\bar{C}_{x2}^{-}C_{x2}'^{-}\tan^2\beta_2 + (U - \bar{C}_{y1})C_{y1}'\right] \tag{30}$$

Nonuniform tangential force and nonuniform pressure can thus be obtained from Eqs. (28) and (30). Upon projection of the tangential force and the pressure forces onto the X, Y axes, the total excitation force coefficients, or the rotordynamic stiffness coefficients, are

$$(\alpha_Y + i\alpha_X)_{\text{total}} = \frac{-\hat{f}_y + iL\langle \hat{P} \rangle}{|\bar{f}_y(e/H)|} \tag{31}$$

The coefficients are composed of contributions from tangential force asymmetry α_{wd} and pressure asymmetry α_P. Forces along the rotor offset are called direct forces and are denoted with a subscript X. Forces perpendicular to the rotor offset are called cross-coupled forces and are denoted with a subscript Y.

III. Model Predictions

This part presents the model predictions for a test compressor. The input flow parameters include the design flow coefficient Φ_D, the design reaction R_D, and the design work coefficient Ψ_D. The input geometry parameters are the mean rotor-tip gap $\bar{t}/H$ and the pitch-chord ratio s/c. Howell's[17] compressor was chosen for this study because $\Phi_D = 0.5$ and $R_D = 0.5$ are common values for compressors. The compressor's parameters are listed in Table 1. $\bar{t}/H$ values of 0.01, 0.02, and 0.04 have been used.

Table 1 Test compressor specification from Howell[17]

Specification	Value
Flow coefficient	0.50
Reaction	0.50
Rotor inlet angle	52.5
Rotor exit angle	35.0
Pitch/chord	1.0

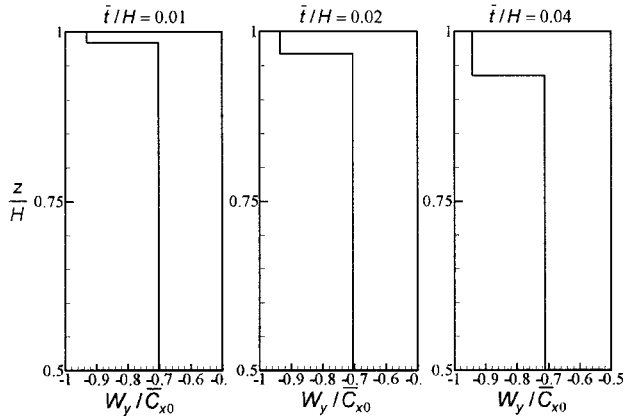

Fig. 6 Radial distribution of relative tangential velocity at rotor exit.

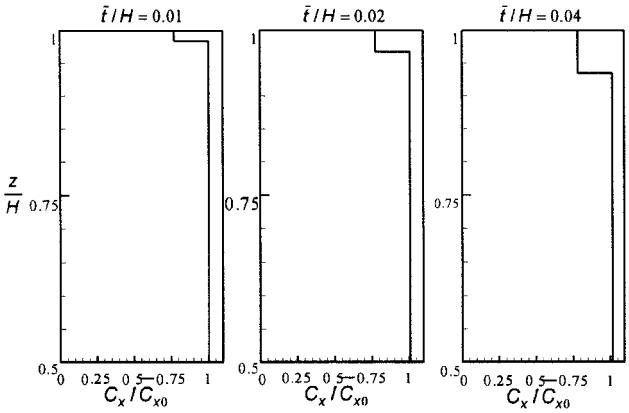

Fig. 7 Radial distribution of axial velocity at rotor exit.

A. Blade Scale Predictions

Figure 6 shows the radial location plotted vs the relative tangential velocity at the rotor exit for three different mean tip clearances. $z/H = 0$ is the hub, $z/H = 1.0$ is the casing wall, and the blade tips are located at $z/H = 0.99$, 0.98, and 0.96. Tangential velocities are considered to be positive in the direction of rotation. In Fig. 6 the relative tangential velocity of the clearance stream (+) has a higher magnitude in the direction opposite to the direction of rotation than that of the passage stream (−). Therefore, relative to the passage stream, the clearance stream is underturned and, thus, has less swirl. In other words, relative to the passage stream, less work is imparted by the compressor onto the stream associated with tip clearance. Figure 7 shows the radial location plotted vs the axial velocity at the rotor exit for three different mean tip clearances. Axial velocity is positive in the downstream direction, and the underturned stream (+) is retarded relative to the passage flow (−) in the axial direction. The figures also show that the defects in swirl and axial momentum of the clearance stream (+) increase with increasing tip clearance. These trends agree with the experimental findings of Hunter and Cumpsty,[18] and the comparison is presented in Roh and Song.[19]

The axial and tangential momentum defects of the clearance stream are essentially caused by tip clearance flow kinematics. As shown in Fig. 4, the underturned stream consisting of the tip clearance flow W_{jet} and passage flow W_{ss} is underturned by angle θ relative to the passage flow. Then, as a result of the flow kinematics,

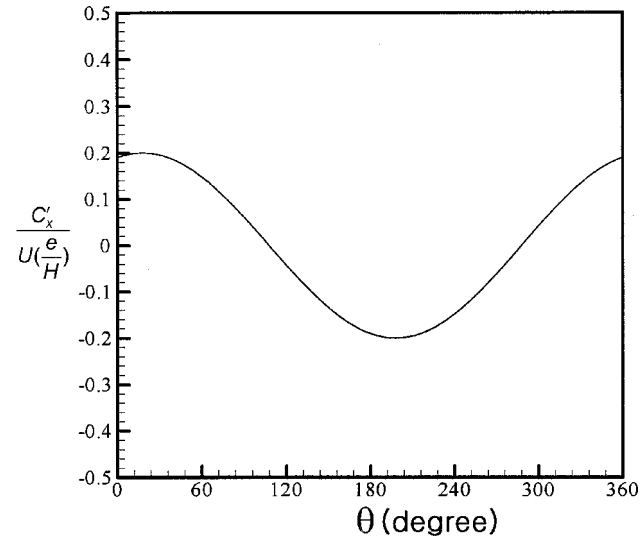

Fig. 8 Upstream axial velocity perturbation (station 0) vs azimuthal angle.

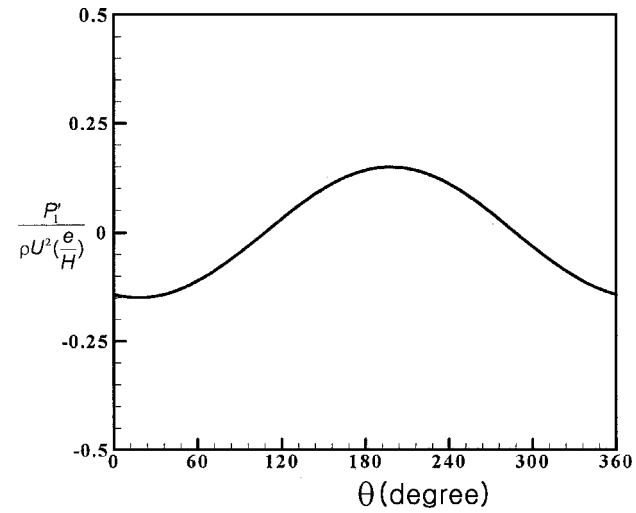

Fig. 9 Upstream pressure perturbation (station 0) vs azimuthal angle.

the underturned stream is retarded in axial direction relative to the passage flow. Thus, the existence of the tip gap forces more flow to go through the blade and loads the compressor.

B. Radius Scale Predictions

Nondimensional flow perturbations, normalized by nondimensional eccentricity e/H, are plotted vs azimuthal location θ in Figs. 8 and 9. The tip clearance is the smallest at $\theta = 0$ deg and the largest at $\theta = 180$ deg. Figure 8 shows the perturbation in axial velocity upstream of the stator (station 0) plotted vs θ. As already discussed, a bigger tip clearance means a higher mass fraction and axial momentum defect of the underturned stream. Therefore, flow migrates azimuthally away from the larger gap toward the smaller gap. Thus, the highest axial velocity occurs near $\theta = 15$ deg. From the Bernoulli relation between $x = -\infty$ and station 0, pressure should be the highest where velocity reaches its minimum. Therefore, the maximum pressure near $\theta = 200$ deg can be seen in Fig. 9.

C. Rotordynamic Coefficient Predictions

For the test compressor the tangential force perturbation is plotted vs azimuthal angle in Fig. 10. The mean value of the nondimensional tangential force $\bar{f}_y/\dot{m}U$ is −0.29. The negative sign signifies that the fluid receives work from the compressor. Also, the negative perturbation near the minimum gap ($\theta = 0$ deg) means that compressor does more work on the fluid in that region. Consequently, the compressor is loaded more highly in the smaller gap region.

Table 2 Predicted excitation force coefficients for the test compressor ($\Phi_D = 0.50, R_D = 0.50$)

Direction	α_p	α_{wd}	α_{total}
X	+1.3	−0.2	+1.1
Y	+0.5	−0.6	−0.1

Table 3 Predicted excitation force coefficients for a turbine ($\Phi_D = 0.58$ and $R_D = 0.21$)[8]

Direction	α_p	α_{wd}	α_{total}
X	−1.8	−0.9	−2.7
Y	+1.4	+1.8	+3.2

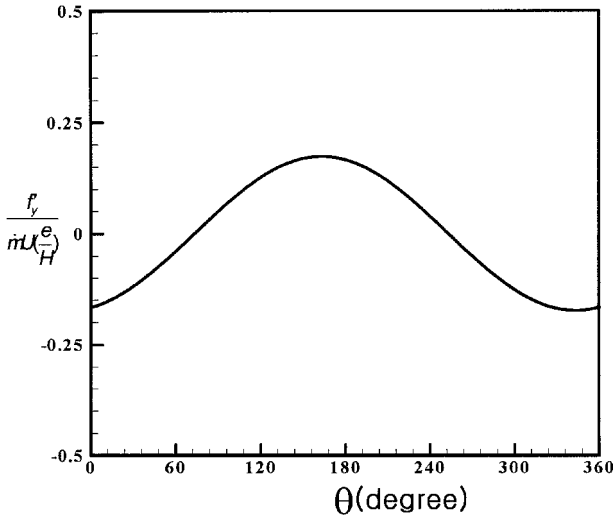

Fig. 10 Tangential force on rotor vs azimuthal angle.

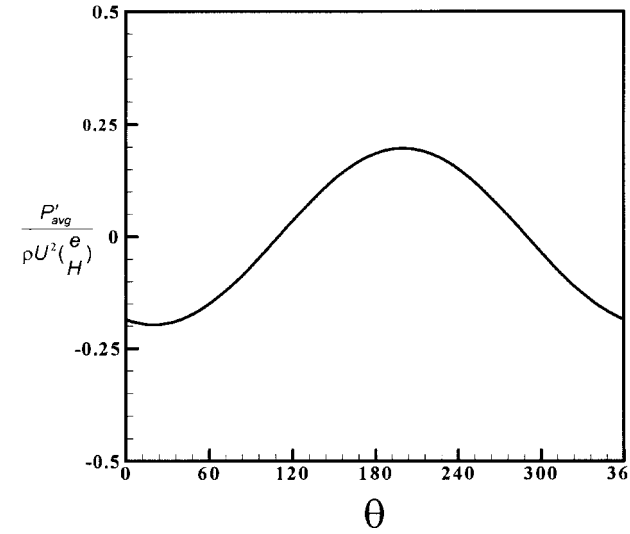

Fig. 12 Perturbation in the average pressure on rotor hub vs azimuthal angle.

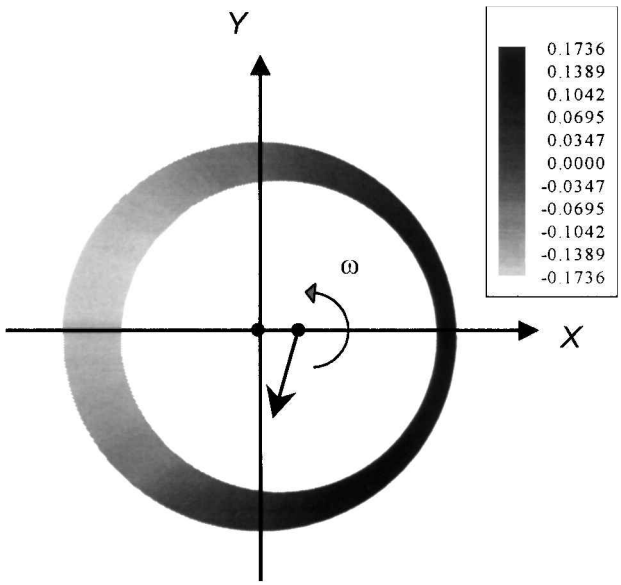

Fig. 11 Schematic of the effect of tangential force asymmetry on compressor rotor.

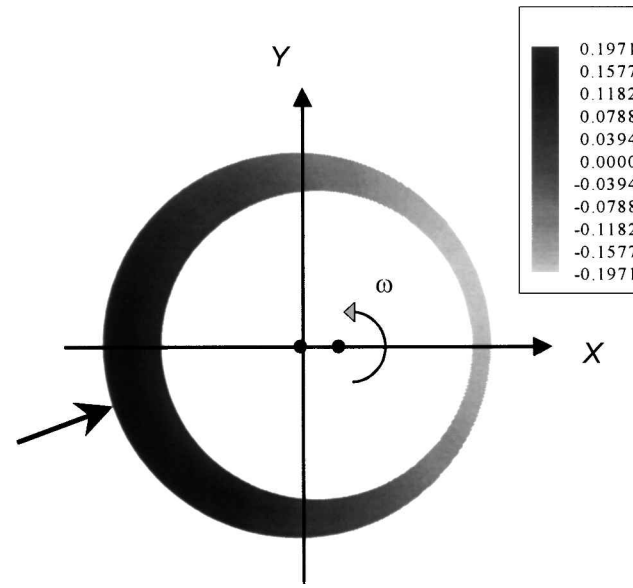

Fig. 13 Schematic of the effect of the average of inlet and exit pressure asymmetry on compressor rotor.

This result is mainly caused by the fact that the mass fraction of underturned stream is the largest near the maximum gap. However, the tangential force in a compressor acts in a direction opposite to that of rotation; therefore, the tangential force asymmetry promotes a backward whirl in compressors (Fig. 11). The forces as a result of the pressure nonuniformity result from the azimuthal flow redistribution caused by the rotor offset. $\langle P \rangle' / \rho U^2 (e/H)$ is plotted vs azimuthal angle in Fig. 12. The maximum pressure is at approximately $\theta = 200$ deg, and, thus, the pressure asymmetry promotes a forward whirl (Fig. 13).

The predicted excitation force coefficients as a result of the tangential force and pressure asymmetries for the test compressor are listed in Table 2. For the direct force the destabilizing pressure effect is approximately twice as large as the stabilizing tangential force effect. Therefore, the total direct force is positive and destabilizing. For the cross-coupled force the magnitude of the forward-whirl-inducing pressure effect is comparable to that of the backward-whirl-inducing tangential force effect. The result is a small backward-whirl-inducing force. These results are for design point operation of the test compressor, and the values would be different for off-design operation and other compressor designs.

For comparison Table 3 lists the coefficient found for a turbine.[8] In magnitude and direction the forces in compressors are different from those in turbines. First, the magnitudes of compressor exictation force coefficients are smaller than those of turbines. This result is caused by the relatively low loading of the test compressor stage, with a loading coefficient value of 0.30, compared to the turbine, with a loading coefficient value of 1.5. Second, the rotordynamic effects of flowfield asymmetries on compressor and turbine are different. In the compressor's case the forces caused by pressure

asymmetry counteract the forces caused by tangential force asymmetry in both X and Y directions. In turbines the situation is different. In the X direction the force caused by pressure asymmetry acts in the same direction as that caused by tangential force asymmetry. However, in the Y direction the forces caused by pressure asymmetry and tangential force asymmetry both act in the same direction.

IV. Conclusions

The main conclusions from this investigation on flow redistribution as a result of rotor-tip clearance in compressors are listed here:

1) An actuator disk model has been newly developed to examine the flow redistribution and rotordynamic effects induced by axisymmetric and nonaxisymmetric rotor-tip clearance in a single-stage axial compressor.

2) In the axisymmetric case, relative to the passage flow, the stream associated with tip clearance is retarded in the axial direction and underturned in the tangential direction.

In the nonaxisymmetric case the following apply:

3) The flow preferentially migrates toward the smaller gap region.

4) Near the larger gap the compressor is loaded more lightly.

5) The direct force caused by pressure asymmetry is positive, whereas that caused by torque asymmetry is negative. Thus, the net direct force is positive.

6) The cross-coupled force caused by pressure asymmetry is positive (inducing a forward whirl), whereas that caused by torque asymmetry is negative (inducing a backward whirl). Thus, the net cross force has a negative sign and a small magnitude.

Acknowledgments

This work was partially supported by Grant 971-1008-050-1 from the Korea Science and Engineering Foundation and by the Institute of Advanced Machinery and Design at Seoul National University.

References

[1]Thomas, H. J., "Unstable Natural Vibration of Turbine Rotors Induced by the Clearance Flow in Glands and Blading," *Bulletin de L'A.I.M.*, Vol. 71, No. 11/12, 1958, pp. 1039–1063.

[2]Alford, J., "Protecting Turbomachinery from Self-Excited Rotor Whirl," *Journal of Engineering for Power*, Vol. 87, Oct. 1965, pp. 333, 334.

[3]Urlichs, K., "Clearance Flow Generated Transverse Forces at the Rotors of Thermal Turbomachines," NASA TM-77292, July 1975 (translation of Ph.D. Dissertation, Munich Technical Univ.).

[4]Martinez-Sanchez, M., Jaroux, B., Song, S. J., and Yoo, S., "Measurement of Turbine Blade-Tip Rotordynamic Excitation Forces," *Journal of Turbomachinery*, Vol. 117, No. 3, 1995, pp. 384–392.

[5]Qiu, Y. J., "An Investigation of Destabilizing Blade Tip Forces for Shrouded and Unshrouded Turbines," M.S. Thesis, Dept. of Aeronautics and Astronautics, Massachusetts Inst. of Technology, Cambridge, MA, Aug. 1985.

[6]Horlock, J. H., and Greitzer, E. M., "Non-Uniform Flows in Axial Compressors Due to Tip Clearance Variation," *Proceedings of the Institution of Mechanical Engineers*, Vol. 197C, 1983, pp. 173–178.

[7]Song, S. J., and Martinez-Sanchez, M., "Rotordynamic Forces due to Turbine Tip Leakage: Part 1—Blade Scale Effects," *Journal of Turbomachinery*, Vol. 119, No. 4, 1997, pp. 695–703.

[8]Song, S. J., and Martinez-Sanchez, M., "Rotordynamic Forces due to Turbine Tip Leakage: Part 2—Radius Scale Effects and Experimental Verification," *Journal of Turbomachinery*, Vol. 119, No. 4, 1997, pp. 704–713.

[9]Vance, J. M., and Laudadio, F. J., "Experimental Measurement of Alford's Force in Axial Flow Turbomachinery," American Society of Mechanical Engineers, Paper 84-GT-140, June 1984.

[10]Colding-Jorgensen, J., "Prediction of Rotordynamic Destabilizing Forces in Axial Flow Compressors," *Journal of Fluids Engineering*, Vol. 114, No. 4, 1992, pp. 621–625.

[11]Ehrich, F. F., "Rotor Whirl Forces Induced by the Tip Clearance Effect in Axial Flow Compressor," *Journal of Vibration and Acoustics*, Vol. 115, No. 3, 1993, pp. 509–515.

[12]Graf, M. B., Wong, T. S., Greitzer, E. M., Marble, F. E., Tan, E. S., Shin, H. W., and Wisler, D. C., "Effects of Nonaxisymmetric Tip Clearance on Axial Compressor Performance and Stability," *Journal of Turbomachinery*, Vol. 120, No. 4, 1998, pp. 648–661.

[13]Cohen, H., Rogers, G. F. C., and Saravanamuttoo, H. I. H., *Gas Turbine Theory*, Longman Scientific & Technical, Essex, England, U.K., 1996, p. 156.

[14]Roh, H. Y., "Blade Scale Effects of Tip Leakage Flow in Axial Compressors," M.S. Thesis, Dept. of Aerospace Engineering, Inha Univ., Inchon, Republic of Korea, Feb. 1997.

[15]Gauthier, R. P., "An Investigation of Flow Field Perturbation Caused by Constant Blade Tip Clearance in a Turbine," M.S. Thesis, Dept. of Aeronautics and Astronautics, Massachusetts Inst. of Technology, Cambridge, MA, June 1990.

[16]Park, K. Y., "Non-Uniform Compressor Flow Fields Induced by Non-Axisymmetric Tip Clearance," M.S. Thesis, Dept. of Aerospace Engineering, Inha Univ, Inchon, Republic of Korea, Feb. 1998.

[17]Howell, A. R., "Design of Axial Compressors," *Proceedings of the Institution of Mechanical Engineers*, Vol. 153, London, 1945.

[18]Hunter, I. H., and Cumpsty, N. A., "Casing Wall Boundary Layer Development Through an Isolated Compressor Rotor," *Journal of Engineering for Power*, Vol. 104, No. 4, 1982, pp. 805–818.

[19]Roh, H. Y., and Song, S. J., "Compressor Tip Clearance Modeling," *Proceedings of the Colloquium on Turbomachinery*, edited by S. J. Song, Turbo and Power Machinery Research Center, Seoul National Univ., Seoul, Republic of Korea, June 1999, pp. 399–405.

J. P. Gore
Associate Editor